JOURNAL OF GEOPHYSICAL RESEARCH, VOL. 90, NO. D5, PAGES 7955–7966, AUGUST 20, 1985

The Response of Ozone to Solar Proton Events During Solar Cycle 21: A Theoretical Interpretation

CHARLES H. JACKMAN AND RICHARD D. MCPETERS

NASA/Goddard Space Flight Center, Atmospheric Chemistry and Dynamics Branch, Greenbelt, Maryland

Substantial ozone decreases at the stratopause and in the mesosphere have now been observed by instruments on the NIMBUS 7 solar backscattered ultraviolet (SBUV) and Solar Mesosphere Explorer (SME) satellites during solar proton events (SPE's) of solar cycle 21. Since the ozone depletion was only observed during the SPE's, we believe that increased production of short-lived HO_x species by protons is responsible for the depletion. We find that one-dimensional time-dependent model calculations are close to agreement with the two satellite instrument measurements in the upper stratosphere and lower mesosphere only when the observed ozone decrease as a function of altitude is used in our model calculations. Most of the ozone depletion between 2 and 0.5 mbar (~45 and 55 km) was caused not by direct particle effects, but by the large ozone decreases at higher altitudes allowing increased penetration of ultraviolet to lower than normal altitudes. Our calculations are qualitatively in agreement with the SBUV measurements but tend to underestimate the ozone depletion for pressure levels between 1 and 0.3 mbar (~50 and 60 km). The calculated ozone depletions at 0.5 and 0.3 mbar (~55 and 60 km) agree fairly well with the observations of SME. The strong solar zenith angle (SZA) dependent depletion that was observed is predicted by the model. Larger SZA's generally reflected larger ozone depletions. However, for SZA's greater than 84° during the July 13, 1982, SPE an ozone decrease less than the ozone decrease at 84° SZA and 1 mbar (~50 km) was predicted by theory and observed in SBUV data. Similar behavior was observed in three other SPE's. As far as we know, this ozone response is the first reported evidence for the much discussed self-healing effect.

INTRODUCTION

Ozone decreases associated with the solar proton event (SPE) that occurred on August 4, 1972, follow approximately the theoretically predicted behavior below 45-km altitude [*Heath et al.*, 1977; *Solomon and Crutzen*, 1981; *Reagan et al.*, 1981]. This was the only SPE documented to cause an ozone depletion below 45 km (~2 mbar). Ozone decreases during the July 13, 1982, and the December 8, 1982, SPE's also follow approximately their theoretically predicted behavior between 60 and 85 km (~0.3 and 0.005 mbar) [*Solomon et al.*, 1983*a*, *b*]. *McPeters et al.* [1981], however, found a substantial ozone loss coinciding with the January 1971 SPE at about 50-km altitude (~1 mbar) that could not be explained by theory. Since there was some concern about proton contamination in the backscattered ultraviolet instrument itself on NIMBUS 4, McPeters et al. noted that observations of SPE's by the NIMBUS 7 solar backscattered ultraviolet (SBUV) instrument, which is insensitive to particles, might confirm these results.

Such SPE's occurred in June and August of 1979, October of 1981, and July and December of 1982. *McPeters and Jackman* [this issue] presented an analysis of the ozone decreases observed during these SPE's. A wide range of proton fluxes was represented in these SPE's, and in spite of nearly an order of magnitude difference in ion pair production between the July 13, 1982, SPE and the August 20–21, 1979, SPE, both SPE's showed some ozone depletion. In this paper we use both a one-dimensional (1D) time-dependent model as well as a 1D photochemical equilibrium model to study these SPE's. The 1D time-dependent model was used to model as realistically as possible the effects of the solar protons on the atmosphere. The 1D photochemical equilibrium model was used for sensitivity studies and also to investigate details of the complex interactive mechanisms ongoing in the atmosphere which lead to ozone changes during SPE's.

During the SPE's of solar cycle 21 in the 2- to 0.5-mbar range (~45–55 km) most of the ozone depletion was not caused by the direct effect of the protons but rather by the ozone depletion above the altitude of interest. Since both the ozone and the molecular oxygen absorption cross sections are significant below about 250 nm, an ozone depletion at any higher level allows both more ozone dissociating solar flux (decreasing ozone below) and more molecular oxygen dissociating solar flux (increasing ozone below) through to lower levels. These competing effects can lead to either an increase or a decrease in ozone at lower altitudes. For most solar zenith angles (SZA's) the ozone depletion above the stratopause results in an ozone decrease at the stratopause; however, at extremely large SZA's, ozone production is enhanced so that our model calculations predict an ozone increase. Because this effect is subtle and maximizes near an SZA of 90° at 2 and 1 mbar (~45 and 50 km), we have only a small amount of observational evidence supporting this theory of self-healing. It appears, however, that the ozone decrease is largest at an SZA of 84° during the July 13, 1982, SPE for an altitude of 1 mbar (~50 km) with smaller amounts of ozone decrease observed at both larger and smaller SZA's.

This observation as well as others lead us to believe that self-healing is possible. Self-healing was first pointed out by H. Harrison in the *Climatic Impact Assessment Program* [1975, pp. 4-24 to 4-36]. This self-healing is similar to the mechanism predicted by theoretical models through which large ozone depletions in the middle to upper stratosphere (that may be brought about by chlorofluoromethanes) are mitigated somewhat by an ozone increase at lower altitudes [*Hudson*, 1977, p. 201]. Confirmation of theoretical model predictions that self-

Paper number 5D0228.

TABLE 1. Ozone (ppmv) Comparison From Models and Satellites

O_3 Time-Dependent Model (84° SZA)	O_3 Photochemical Equilibrium Model (84° SZA)	O_3 NIMBUS 7 SBUV (84.3° SZA)	O_3 SME (A.M. Node of Orbit)
3.31 (2.24 mbar)	2.59 (45 km, 1.82 mbar)	4.27 (2 mbar)	
2.34 (1.27 mbar)	2.05 (50 km, 0.99 mbar)	2.49 (1 mbar)	2.72 (50 km)
1.25 (0.54 mbar)	1.29 (55 km, 0.54 mbar)	1.35 (0.5 mbar)	1.75 (55 km)
0.78 (0.31 mbar)	0.77 (60 km, 0.29 mbar)	0.84 (0.3 mbar)	1.18 (60 km)

healing does occur in the atmosphere is another convenient test to prove model validity.

ENERGY DEPOSITION BY SOLAR PROTONS AND ELECTRONS

Proton fluxes were measured by the IMP 8 and NOAA 6 satellites during solar cycle 21. For SPE's other than the July 13 and December 8, 1982, events, the solar proton flux data were taken from IMP 8 measurements. Information from Solar Geophysical Data (1980) was used for SPE's in the time frame of June 1979 through September 1979. These proton fluxes were measured in energy bins 0.97–1.85, 4.0–12.5, 13.7–25.2, 20–40, and 40–80 MeV. R. E. McGuire (private communication, 1983) provided proton fluxes for the October 13–14, 1981, and the January 31, 1982, SPE's, with the protons being measured in bins 4.20–8.65, 8.65–22.50, 19.80–28.74, 28.74–42.90, 42.93–81.00, and 107.30–154.50 MeV. The NOAA 6 satellite measured both proton and electron fluxes for the July 13 and December 8, 1982, SPE's. These data were provided to us by D. Evans and H. Sauer (NOAA) through S. Solomon (NOAA) and contain information for protons at energies >16, >32, and >80 MeV and for electrons at energies >30, >100, and >300 keV.

Hourly average proton and electron (where provided) spectra were constructed with a series of exponential energy segments fitted to the data. Ionization rates between 40 and 100 km were then calculated for the protons by the method outlined in *Jackman et al.* [1980] and for the electrons by the method outlined in *Goldberg et al.* [1984]. We will not go into the details of the energy degradation calculations but offer this short description: the protons and electrons impinge into the atmosphere isotropically at 35 different angles and degrade their energy following well-known range energy relations. Time- and altitude-dependent ionization rates were calculated for the following SPEs: June 7, 1979, August 20–21, 1979, September 17, 1979, October 13–14, 1981, January 31, 1982, July 13, 1982, and December 8, 1982. The time- and altitude-dependent ionization rates for most of these SPE's are given in Figures 2–7 of *McPeters and Jackman* [this issue].

The electron ion pair production was less than 10% of the proton ion pair production during the two SPE's (July 13 and December 8, 1982), where both the electron and proton flux data were available. The electrons are therefore relatively unimportant regarding total energy deposition.

PHOTOCHEMISTRY

The positive ions produced by the solar protons and electrons form ion water clusters and, subsequently, H and OH. The complex ion chemistry leading from the ion water clusters to the HO_x species has been discussed before by *Swider and Keneshea* [1973], *Frederick* [1976], *Crutzen and Solomon* [1980], and *Solomon et al.* [1981]. Below 70 km, most of the positive ions result in the formation of two HO_x species apiece. Above 75 km the HO_x produced per positive ion is somewhat less than 2 and is also strongly altitude dependent [*Solomon et al.*, 1983*a*].

In this paper we are concerned with altitudes at and below 60 km, and we assume that two HO_x species are produced per positive ion. The major O_x destruction reactions from Table A1 connected with HO_x between 45 and 60 km ($\sim$2 and 0.3 mbar) are

$$\text{(R18)} \qquad O + OH \rightarrow H + O_2$$

$$\text{(R20)} \qquad O + HO_2 \rightarrow OH + O_2$$

We will not go into the catalytic cycles connected with O_x destruction by HO_x, but refer the reader to Nicolet [1975] or *Johnston and Podolske* [1978] for a rather complete discussion. An analytic formula relating HO_x production to O_x destruction is given in *Solomon et al.* [1983*a*], who note, however, that the formula is only valid near 70 km. Although the NO_x produced by the SPE's is substantially less important than the HO_x at our altitudes of interest, we do include its production and assume that 1.25 NO molecules are produced per ion pair [*Jackman et al.*, 1980; *McPeters et al.*, 1981].

As noted in *McPeters et al.* [1981], implied in *Swider and Keneshea* [1973], *Frederick* [1976], and *Swider et al.* [1978], and subsequently observed and confirmed in *Thomas et al.* [1983] and *Solomon et al.* [1983*a*], an SPE should have its maximum effect at the highest SZA's.

The natural source of HO_x is

$$N_{HO_x} = 2J_4[H_2O] + 2k_{27}[O(^1D)][H_2O] \qquad (1)$$

The factor of 2 arises in each of the terms because two HO_x species are produced as a result of reactions (R4) and (R27). Below 70 km the SPE source of HO_x species is

$$S_{HO_x} = 2q_{ION} \qquad (2)$$

where q_{ION} is the rate of production of positive ions. The total HO_x source during an SPE is

$$T_{HO_x} = N_{HO_x} + S_{HO_x} \qquad (3)$$

Increasing the SZA leads to a decrease in the $O(^1D)$ concentration and a decrease in the J_4, and subsequently, a decrease in the natural HO_x source, N_{HO_x}. The SPE HO_x source, S_{HO_x}, is essentially unchanged during a change in the SZA; consequently, the influence of the SPE is increased.

MODEL DESCRIPTION

We use two 1D models to study this atmospheric problem. The 1D time-dependent model brings in a more complete chemistry as well as a more realistic portrayal of the atmosphere during an SPE at a particular point. The 1D photochemical equilibrium model, while not as realistic as the time-dependent model, does offer the flexibilities of a simpler model. This simpler model was used for sensitivity studies and

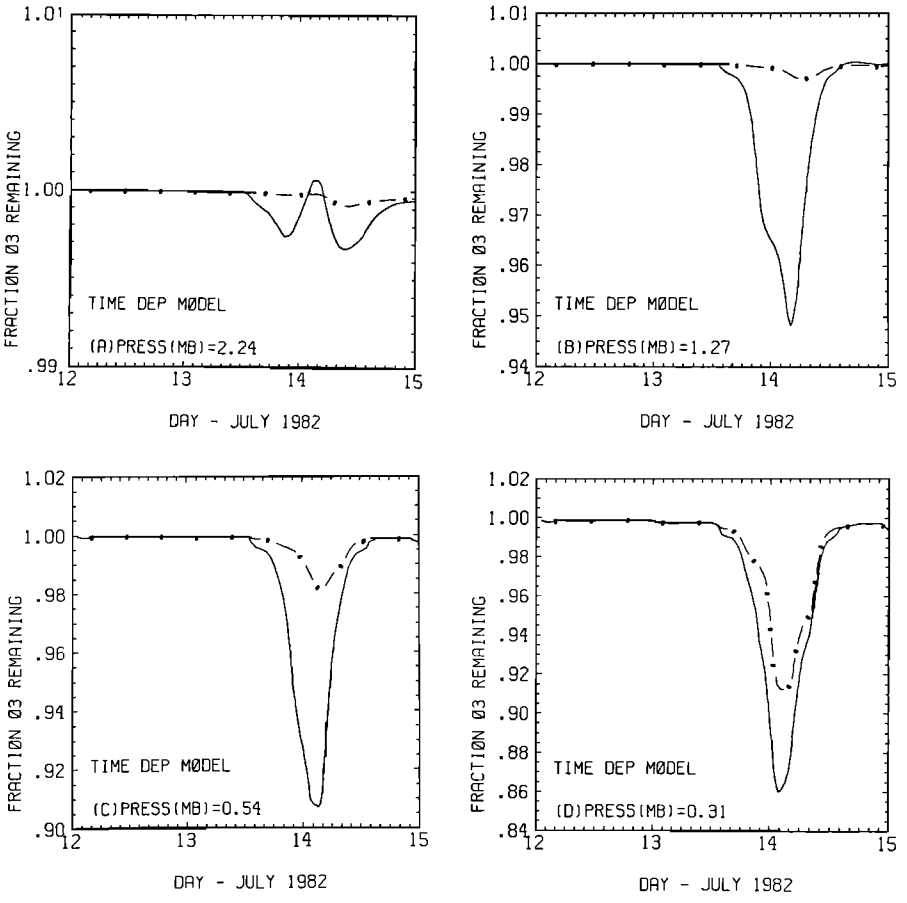

Fig. 1. One-dimensional time-dependent model calculations of ozone depletion for the July 13, 1982, SPE. The dash-dot line denotes model-predicted fraction ozone remaining assuming a totally self-consistent model. The solid line denotes model-predicted fraction ozone remaining assuming ozone depletion above commensurate with the observations.

also studies to investigate the details of the very complex interactive photochemical mechanisms ongoing during SPE's. Both models are described in the appendix.

Since most of the observed ozone changes occur when the SZA is greater than 70°, the radiation field for a spherical atmosphere in both 1D models must be handled correctly with the use of the Chapman function. We use the formulation of *Smith and Smith* [1972] in order to evaluate the Chapman function. This Chapman function assumes an exponentially decreasing atmosphere and thus only requires a scale height for the species of interest and the altitude of the point of consideration. The two important species involved in calculating the optical depth in this region of the atmosphere are O_2 and O_3. The scale height for O_2 is about 7 km and the computed scale height for O_3, using the ambient measurements of NIMBUS 7 (SBUV) and the Solar Mesosphere Explorer (SME), is 5.5 km. An exponentially decreasing O_3 is a good assumption in the upper stratosphere and lower mesosphere. The solar flux at any point can be calculated using

$$F(z)_i = F(\infty)_i \exp\left[-ch(X, z, O_2)\sigma(O_2)N(O_2)_i - ch(X, z, O_3)\sigma(O_3)N(O_3)_i\right] \quad (4)$$

where $F(z)_i$ (photons cm^{-2} s^{-1}) is the solar flux in the ith wavelength region at altitude z, $F(\infty)_i$ is the solar flux in the ith wavelength region at the top of the atmosphere; $ch(X, z, O_2)$ and $ch(X, z, O_3)$ are the Chapman functions for O_2 and O_3, respectively, at a solar zenith angle X and altitude z; $\sigma(O_2)_i$ and $\sigma(O_3)_i$ are the photoabsorption cross sections (cm^2) for O_2 and O_3, respectively; and $N(O_2)$ and $N(O_3)$ are the vertical column densities (cm^{-2}) for O_2 and O_3, respectively. It is readily seen that any changes in $N(O_3)$ can cause extremely large changes in the solar flux at the point of interest, especially for large SZA's.

In Table 1 we compare the ozone from the two models to the observations by both the NIMBUS 7 (SBUV) and the SME satellites. We compare a base run of both models to ambient ozone values observed. The 1D time-dependent model has a height grid based on pressure, whereas the 1D photochemical model has a height grid based on altitude. The two models agree fairly well with each other, especially at altitudes of 55 and 60 km (~0.5 and 0.3 mbar), where it is assumed that the region is photochemical. The two models agree less well at lower altitudes, but part of that difference is because the ozone values are shown at slightly different altitudes. Other differences between the two models include (1) the 1D time-dependent model is imbedded in a two-dimensional model with the ozone field fixed to NIMBUS 7 (SBUV) values at all but the 1D point and (2) the 1D time-dependent model has a more extensive chemistry set included.

The two models agree fairly well with the measurements, although at all heights the models compute a smaller ozone amount than is actually observed. This underprediction of ozone amount has been observed before in other model calculations [*Solomon et al.*, 1983c; *Crutzen and Schmailzl*, 1983]. In spite of this disagreement between the absolute values of ozone computed in the models and observed in the atmosphere, the calculations of fraction of ozone remaining during

the SPE should be comparable for the models and observations.

MODEL RESULTS

We use the 1D time-dependent model to calculate the fraction of ozone remaining at four pressures, 2.24, 1.27, 0.54, and 0.31 mbar, for the July 13, 1982, SPE. The HO_x production from the solar protons is assumed to be equal to 2 times the ion pair production. The NO_x production from the solar protons is assumed to be equal to 1.25 times the ion pair production. We set the latitude at 68.7°, so the maximum SZA on July 13 would be at 89°. The maximum proton intensity in the July 13, 1982, SPE occurred at about 1700 UT. In order to maximize the effect of the SPE, we required the maximum intensity of the SPE to coincide with local midnight (maximum SZA). The requirement implied that the longitude of interest was 105°E.

In Figure 1 we present the results of this calculation. First a run was completed for days July 12–14, 1982, in which no solar protons were present. This run was called the "quiescent run." Subsequent runs were compared by taking the ratio of the ozone values of "perturbed runs," which had solar protons included, to this quiescent run. The dash-dot line represents the results of a perturbed run that is totally self-consistent. The ozone depletion above a point comes solely from the computation of ozone decrease arising from the model results. The solid line represents a computation that is not self-consistent but is probably more realistic because it includes the large ozone changes observed. The ozone depletion above each point comes from observations using the NIMBUS 7 (for 2–0.5 mbar) and SME (for 0.3 mbar on up) satellites.

In Figure 1*a* for a pressure of 2.24 mbar the totally self-consistent run shows only a slight decrease during the SPE (note the small range of the ordinate scale). In the more realistic run a decrease is obtained commencing with the start of the SPE. An upturn was computed beginning in the evening hours of July 13 and peaking in the early morning hours of July 14. The amount of ozone actually reaches a value that is larger than that calculated in the quiescent run. This effect is referred to as self-healing, where the ozone amount at a point is increased due to an ozone depletion above, and will be discussed later.

The totally self-consistent perturbed run (represented by the dash-dot line) in Figure 1*b* for a pressure of 1.27 mbar shows only a slight decrease during the SPE. The more realistic perturbed run, explained above, shows close to a factor of 10 larger decrease. Note the slight kink in the solid curve in the late evening hours of July 13. This is probably also related to the self-healing effect.

The more realistic run for 0.54 mbar given in Figure 1*c* again shows a much larger ozone decrease than that calculated in the totally self-consistent perturbed run. A similar pattern is present in Figure 1*d* for 0.31 mbar, but not to the extent obtained for the other three pressure levels. Note that most of the ozone depletion occurs during the time of the SPE itself. At these heights HO_x is the dominant species in determining the ozone amount and has a lifetime on the order of hours. It was concluded and verified that the solar proton production of HO_x was the dominant mechanism for ozone depletion. The slight amount of residual ozone change at the beginning of July 15, computed for all four pressure levels with the 1D time-dependent model, is the decrease in ozone resulting from the longer lived NO_x species that were also produced during the SPE.

Since the 1D time-dependent model is a computation for one geographic point over the entire time of the SPE, it is difficult to relate this computation directly to the observations by the two satellites, NIMBUS 7 and SME. The two satellites observed the same geographic point at the very high latitudes approximately every 12 hours, because these latitudes are sunlit 24 hours a day in the summer. Most of the protons associated with the July 13, 1982, SPE interacted with the earth's atmosphere in a time less than 24 hours; therefore such a direct comparison was difficult. We use results of this model in conjunction with results of the 1D photochemical equilibrium model to discuss the ozone behavior during this SPE.

We now consider the observations of the two satellites. There have been enough data from these satellites to define a very definite SZA dependence (first pointed out in *Thomas et al.* [1983] and *Solomon et al.* [1983*a*]). In Figure 2 the observations from both satellites are presented on the same graphs. The N's in Figure 2 represent the measurements by the SBUV instrument on NIMBUS 7. The X's denote data from the ultraviolet spectrometer and the O's denote data from the near-infrared spectrometer, both instruments on SME [*Thomas et al.*, 1983]. Ozone data at SZA's below 80° at 0.3 mbar (~60 km) are not possible with the SBUV instrument.

It is apparent from Figure 2 that the two satellites do not always agree on the ozone depletion observed. The SBUV measurements show a larger ozone depletion at altitudes 50, 55, and 60 km (~1, 0.5, and 0.3 mbar) for SZA's greater than 75°. There is a difference in the local time of observation by the two satellites for a given SZA. Near an SZA of about 80° the SME observed at a local time near 5 A.M. and NIMBUS 7 (SBUV) observed at a local time near 2 A.M. The SPE changes its intensity with time [see *McPeters and Jackman*, this issue, Figure 2], and a large SZA influence is expected. It is not surprising therefore that the SBUV and SME instruments observe a different ozone depletion.

On these same graphs we present our results from the 1D photochemical equilibrium model. We use the ion pair production rate at the maximum of the SPE in these model studies. The HO_x production due to the SPE (2 times the ion pair production) is simply added to the ambient HO_x production and is assumed to be constant. This assumption results in an overestimate of the ozone depletion from the model calculations.

The NO_x production due to the SPE is added in a simplified manner. Since NO_x has a long lifetime compared with the duration of the SPE, the NO_x enhancement is calculated by multiplying the NO_x production rate (1.25 times the ion pair production rate) times 12 hours (an assumed average time of maximum intensity for the SPE) and adding this value to the ambient NO. Even with this crude approximation, which overestimates the NO_x produced during an SPE, the ozone decrease due to SPE NO_x production is never more than 0.3% at any altitude for any SZA during the July 13, 1982, SPE.

Since there is an observed O_3 decrease due to the SPE as a function of SZA and height, we use the observed O_3 decrease (as we did in one of the perturbed runs with the 1D time-dependent model) to get out more realistic photodissociation rates for both O_3 and O_2. With this approach the 1D photochemical equilibrium model was employed to derive the lines given in Figure 2. The maximum decrease predicted is about 1% at 45 km (~2 mbar), 5.5% at 50 km (~1 mbar), 12% at 55 km (~0.5 mbar), and 28% at 60 km (~0.3 mbar). These results can be compared with the maximum ozone decreases

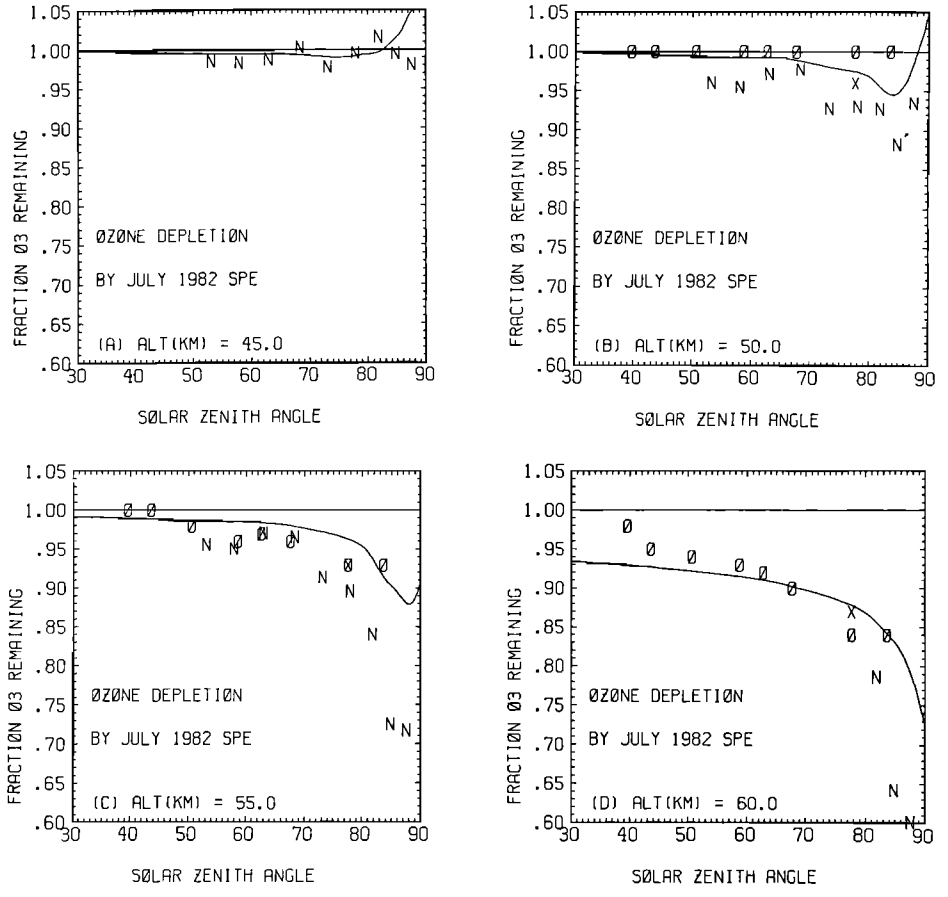

Fig. 2. Observations (points) of ozone depletion for the July 13, 1982, SPE and comparison with model results (solid lines) for (*a*) 45 km, (*b*) 50 km, (*c*) 55 km, and (*d*) 60 km. The N's represent SBUV data, the X's SME ultraviolet spectrometer data, and the O's SME near-infrared spectrometer data. Solid line denotes one-dimensional photochemical equilibrium model-predicted fraction ozone remaining assuming ozone depletion above commensurate with the observations. For clarity, the ordinate value of 1.0 is designated across the figure.

computed with the use of the 1D time-dependent model, which are about an 0.3% decrease at 2.24 mbar, 5.5% at 1.27 mbar, 9% at 0.54 mbar, and 14% at 0.31 mbar. At all heights the 1D photochemical equilibrium model results give the same or larger ozone decrease than that computed in the 1D time-dependent model, which is not unexpected. The results from the two models are close enough, however, that the 1D photochemical equilibrium model results can be compared with the satellite observations with some confidence, especially at 55 km and below.

The 1D photochemical equilibrium model results are closest to the measurements of SME but give less ozone depletion than that seen in the SBUV measurements. For example, at 0.3 mbar (~60 km) and 84.3° SZA the SBUV observations indicate a 36% decrease, while the model suggests a 16% decrease.

One curious feature of the theoretical curve in Figures 2*a*–2*c* is the upturn at very high SZA's. This upturn even goes positive for SZA's greater than 88° at 50 km and for SZA's greater than 82.5° at 45 km (see Figures 2*a* and 2*b*). This self-healing effect has been obtained before in models, mainly when dealing with the lower stratosphere [see, e.g., *Hudson*, 1977, p. 201]. The self-healing is obtained at these higher altitudes because we are dealing with column O_3 and O_2 at large SZA's, which are similar in magnitude to the column O_3 and O_2 at lower altitudes and smaller SZA's. At smaller SZA's these large optical depths for ultraviolet solar flux penetration would only be obtained at much lower altitudes.

Solar Zenith Angle Effect

To help in understanding mechanisms that lead to the SZA-dependent ozone depletion, we need to look at the photodissociation rates (J coefficients) for O_2 and O_3 and how they change as a function of a change in $N(O_3)$. To a good approximation, the continuity equation for odd oxygen (O_x) between 45 and 60 km can be written

$$\frac{d[O_x]}{dt} = 2J_1[O_2] - 2k_{17}[O_3][O] - k_{18}[OH][O] - k_{20}[HO_2][O] - 2k_{25}[NO_2][O] - 2k_{31}[ClO][O] \quad (5)$$

We assume photochemical equilibrium for O_x and for atomic oxygen; thus

$$[O] = \frac{(J_2 + J_3)[O_3]}{k_{16}[O_2][M]} \quad (6)$$

If we substitute the right-hand side of (6) into (5) for [O] and take the derivative of (5) with respect to the column change in

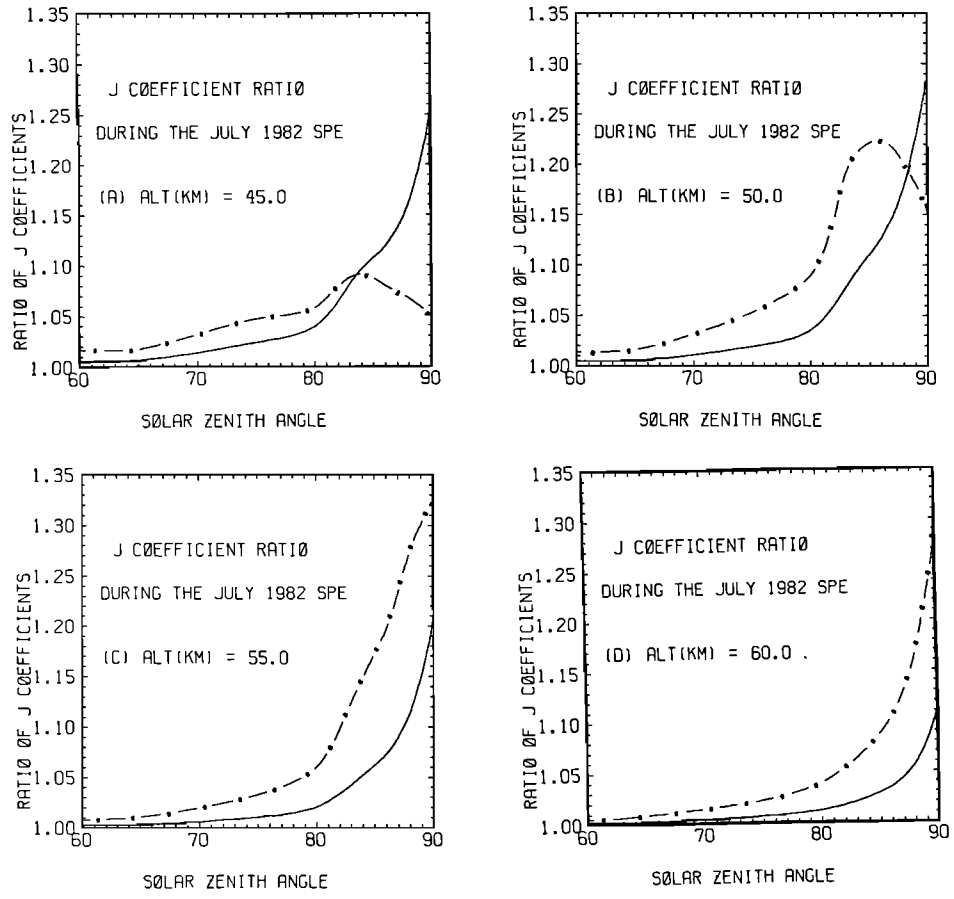

Fig. 3. One-dimensional photochemical equilibrium model calculations of J coefficient ratios for O_2 (solid line) and O_3 (dash-dot line) at (*a*) 45 km, (*b*) 50 km, (*c*) 55 km, and (*d*) 60 km. The ratios are calculated by dividing the J coefficients computed during the July 13, 1982, SPE by the J coefficients calculated during a quiescent time.

O_3, then we derive

$$\frac{d[O_3]}{dN(O_3)} = \left(\frac{AdJ_1}{dN(O_3)} - \frac{Bd(J_2 + J_3)}{dN(O_3)}\right)C^{-1} \tag{7}$$

where

$$A = 2k_{16}[O_2][O_2][M]$$

$$B = [O_3](2k_{17}[O_3] + k_{18}[OH] + k_{20}[HO_2] + 2k_{25}[NO_2] + 2k_{31}[ClO])$$

$$C = (J_2 + J_3)(4k_{17}[O_3] + k_{18}[OH] + k_{20}[HO_2] + 2k_{25}[NO_2] + 2k_{31}[ClO])$$

Included in the derivation of (7) are the simplifying assumptions that the derivatives of species, other than O_3, to a change in $N(O_3)$ are zero. In reality, both HO_x species will change because of the changing $N(O_3)$ influencing the radiation field. This should be a second-order effect. It is clear from (7) that decreases in the $N(O_3)$ can result in decreases or increases in $[O_x]$, and ultimately $[O_3]$, depending on which term dominates on the right-hand side of the equation.

Ozone and molecular oxygen compete for solar photons at wavelengths below 250 nm. At large SZA's ozone removes a large part of the solar flux in the Hartley continuum between 222 and 296 nm. The solar flux at wavelengths larger than 296 nm is not substantially changed at large SZA's. Reflection does become increasingly important but affects all wavelengths similarly in our model representation. The solar flux is reduced at large SZA's below 222 nm, but not as much as in the Hartley continuum. Ozone receives a significant contribution to its photodissociation rate from solar fluxes above 296 nm, and at increasingly larger SZA's this contribution is increased even more as the Hartley continuum contribution is reduced. Therefore near the stratopause at the highest SZA's, changes in ozone above a certain altitude will not substantially influence the ozone photodissociation rate at that altitude. These changes in ozone will, however, substantially influence the molecular oxygen photodissociation rate, as it has no photodissociation above wavelengths of 250 nm.

One good way to examine the behavior of the photodissociation rates (J coefficients) for O_2 and O_3 is to graph a ratio of the rates before and after a change in $N(O_3)$. We do this with the use of our 1D photochemical equilibrium model. The ratio is found by dividing the J's calculated assuming a July 13, 1982, SPE-related O_3 decrease above the altitude of interest by the J's calculated assuming a quiescent state of the atmosphere. These ratios are given in Figure 3 for altitudes 45, 50, 55, and 60 km. At an altitude of 45 km the ratio of the O_3 total J coefficient, $R_{J_2+J_3}$ (represented by the dash-dot line), is larger than the ratio of the O_2 total J coefficient, R_{J_1} (represented by the solid line), for SZA's below about 83.5°. For SZA's above 83.5°, however, just the reverse is true and R_{J_1} increases most dramatically. At 50 km the crossover occurs at the higher SZA of about 88°, and at 55 and 60 km, $R_{J_2+J_3}$ is always higher than R_{J_1}. The J coefficients for both O_2 and O_3 increase with decreasing $N(O_3)$. The net effect on ozone does

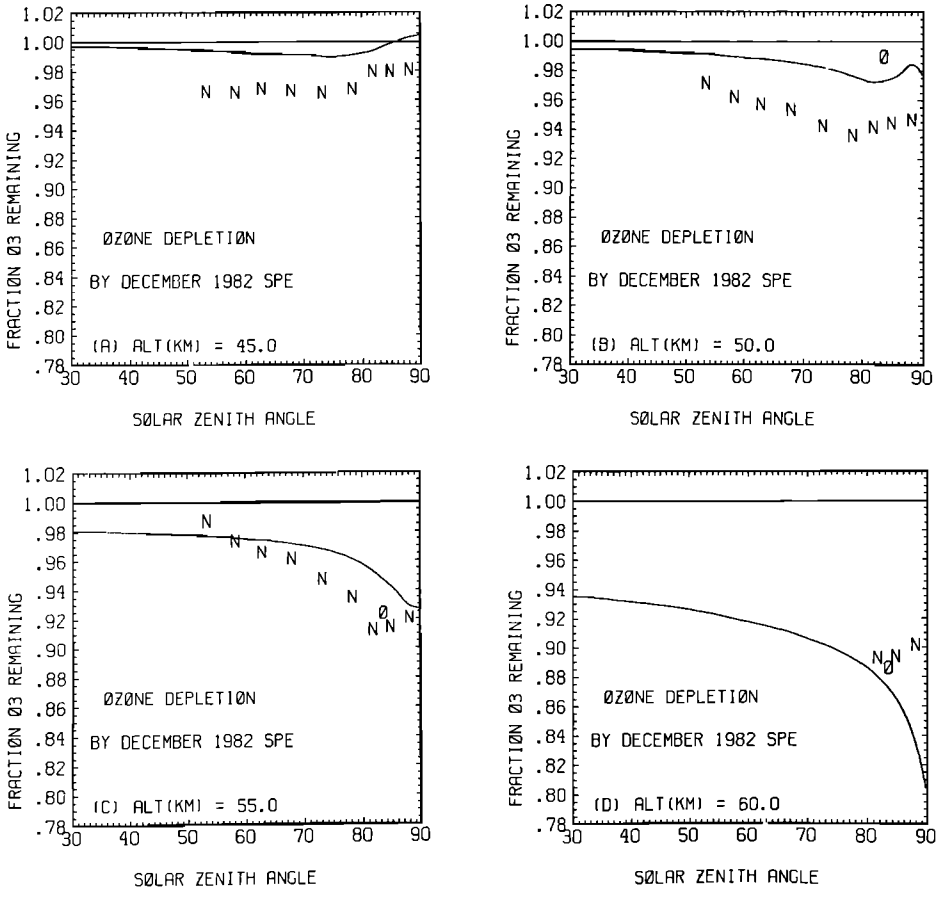

Fig. 4. Observations (points) of ozone depletion for the December 8, 1982, SPE and comparison with model results (solid lines) for (*a*) 45 km, (*b*) 50 km, (*c*) 55 km, and (*d*) 60 km. The lines and points are as described in Figure 2. For clarity, the ordinate value of 1.0 is designated across the figure.

not depend solely on whether the J coefficients increase or decrease but on how much the J coefficients increase or decrease at a particular point.

The SBUV observations at 2 mbar for the July 13, 1982, SPE show no depletion outside the $\pm 2\%$ uncertainty in the data and show little, if any, SZA-dependent ozone depletion (shown in Figure 2*a*). Our 1D photochemical equilibrium model predicts self-healing at 45 km (~ 2 mbar) for SZA's above 82.5°. Our 1D time-dependent model predicts self-healing at 2.24 mbar for SZA's near 80°; however, it is quite subtle.

At 50 km (~ 1 mbar) our 1D photochemical equilibrium model predicts a maximum ozone depletion at an SZA of 84° and significantly less depletion at 88°. Our 1D time-dependent model shows a change in shape between 85° and 89° SZA at 1.27 mbar, which is probably connected with self-healing. Also, in the 1D time-dependent model the maximum SZA does not necessarily correspond to the SZA at which the maximum depletion occurs. This holds true in spite of the fact that the maximum ionization rate occurs at the maximum SZA. At 1.27 mbar, for instance, the maximum ozone depletion occurs at an SZA of 80°. There is scatter in the SBUV observations at 1 mbar but the maximum ozone depletion does occur at an SZA of about 84° (shown in Figure 2*b*). This is our best evidence of the reality of self-healing, observationally.

Normally, ozone profiles from SBUV are calculated only to a maximum SZA of 86°, primarily because the accuracy of the total ozone retrieval cannot be guaranteed for higher SZA's. In order to verify the model prediction of a self-healing effect at 88° SZA, we extended the SBUV ozone profile retrieval to 89° SZA for the July 13 and December 8, 1982, SPE's. The profile retrieval incorporates a spherical shell atmosphere model, so the profiles should be fairly accurate; more important, the ratio of ozone during the SPE to the non-SPE ozone should be quite accurate. These results for an 86°–89° SZA zone are plotted in Figure 2.

A rather large increase in ozone depletion is predicted by the 1D photochemical equilibrium model between SZA's of 70° and 88° at 55 km. However, the amount of predicted ozone decrease is reduced at SZA's above 88°. SBUV observations at 0.5 mbar show a similar enhancement of ozone depletion between 70° and 84° but then show a trailing off with only a slight increase in ozone depletion between 84° and 87° (shown in Figure 2*c*). At 50 km (Figures 1*b* and 2*b*), 55 km (Figures 1*c* and 2*c*), and 60 km (Figures 1*d* and 2*d*) both models tend to underpredict the ozone depletion observed by SBUV. The 1D photochemical equilibrium model predictions tend to be quite close to the SME observations at most SZA's for altitudes of 50, 55, and 60 km. The model results and observations therefore appear to be in fair agreement as long as the observed ozone depletion is used in the model calculations.

Could the ozone depletion behavior as a function of SZA be observed in other SPE's? We looked at other SPE's in solar cycle 21 to determine the answer to this question. The background ozone data were much less variable during December

1982 than during July 1982. The observed ozone depletion and model calculations are plotted for this event in Figure 4 for the four altitudes 45, 50, 55, and 60 km. The observations are labeled the same as in Figure 2 with the SME results coming from *Solomon et al.* [1983*b*]. Again the curve is from the 1D photochemical equilibrium model calculations assuming ozone depletion above the altitude of interest. There is some evidence at 45 km in the SBUV data of the observed ozone decrease becoming less at the higher SZA's and also even a hint of this effect at 50, 55, and 60 km. The 1D photochemical equilibrium model gives approximately the correct shape for the SZA dependence but predicts a lower amount of ozone depletion than that observed at most altitudes. At 60 km the predicted ozone depletion is more than that which is observed. We performed a similar calculation with our 1D time-dependent model. This model predicted an amount of ozone depletion lower than the amount of ozone depletion observed at all altitudes from 2.24 up to 0.31 mbar (~45 up to 60 km), even when the observed ozone depletion above the altitude of interest was used in the calculations. Other SPE's, namely, those that occurred in August of 1979 and October of 1981 show some evidence of self-healing at 45 km. Thus based on these four SPE's, we believe that this solar zenith angle behavior, although subtle, is real.

THREE SOLAR PROTON EVENTS DURING SOLAR CYCLE 20

Measurements of ozone decrease at very large SZA's have been made during other SPE's. *Weeks et al.*, [1972] made measurements from rockets during and after the SPE in November 1969. They observed substantial ozone depletions down to 52 km at an SZA of 89.8°. We have also put the necessary parameters for this SPE into our 1D photochemical equilibrium model, namely, the ambient ozone up to 90 km, the ozone decrease seen during the SPE, and the maximum ion pair production using Solar Geophysical Data (1970) and our proton degradation method. Again our model ozone decrease predictions are lower than the ozone depletions observed. At 55 km the model predicts an ozone decrease of 33%, whereas the observations indicate a 53% depletion. At 60 km the model gives a depletion of 34% and the observations give 68%. The January and September 1971 SPE's were also observed to produce an ozone depletion at fairly large SZA's (75°–80°). The ozone depletion predicted with our model is, again, smaller than that which is observed.

SENSITIVITY STUDIES

A rather extensive sensitivity study was undertaken by *McPeters et al.* [1981] to investigate the possibility of obtaining a larger ozone depletion for a given ionization rate, and will not be repeated here. In this study we obtain essentially the same result as that given in our earlier paper in spite of some changed reaction rates between the *Hudson and Reed* [1979] reaction rate list and the *National Aeronautics and Space Administration* [1983] reaction rate list. The result is at 1 mbar a totally self-consistent model calculation for ozone depletion resulting from an SPE underestimates by a substantial amount the ozone depletion actually observed via a satellite measurement.

One of the significant conclusions of this paper is that the ozone decrease above a point can cause an ozone decrease at that point. Thus using a more realistic model, which contains the ozone depletion measurements above a particular point as part of the calculation, we obtain an ozone depletion prediction at that point which is closer to the observations.

Since some of the species are fixed in our 1D model computations, we performed several sensitivity studies with the use of the 1D photochemical equilibrium model. We varied the amounts of certain species in these studies. In particular, we halved H_2O, NO, and Cl_x and doubled H_2O, NO, and Cl_x in six separate runs. The ozone changed in the quiescent state for each of the runs; the ozone increased for the halved H_2O, NO, and Cl_x cases, and the ozone decreased for the double H_2O, NO, and Cl_x cases. In certain cases the quiescent state ozone changed by a substantial amount, up to 30%. In comparing these sensitivity runs at 50 km the ozone is decreased at an SZA of about 84° by a range of 4–6.5%. The observations of ozone depletion by NIMBUS 7 (SBUV) show a decrease of about 12% at this SZA.

We also performed a sensitivity study of the scale height used in computation of the Chapman function for ozone. We used both a 3.5- and a 7.5-km scale height in two sensitivity runs. Although the quiescent ozone was changed slightly at the very highest SZA's, the computed ozone decrease was changed very little.

We thus conclude that our computations are fairly robust and conclusions fairly valid for most species' changes and ozone scale height changes. An ozone depletion from a self-consistent model calculation more in agreement with the satellite observations could probably be found by varying reaction rates and species' concentrations within their uncertainties. It is doubtful, however, that the solution would be unique or, more important, correct.

TEMPERATURE EFFECT

Temperature decreases in the ambient temperature field should result in ozone increases at 45 km and above, the two being anticorrelated [*Barnett et al.*, 1975] because of the temperature-dependent photochemical reaction rates. Ozone decreases brought about by a nontemperature-dependent perturbation to the atmosphere such as an SPE should result in temperature decreases because ozone photolysis causes direct heating of the middle atmosphere. Substantial ozone decreases observed during SPE's of solar cycle 21 occurred only at the highest SZA's. Also, since heating rates at 50 km (~1 mbar) are on the order of about 10° K/d [*Schoeberl and Strobel*, 1978], it would take a significant change in the ozone over a day to decrease the temperature perceptibly. We have looked at National Meteorological Center (NMC) temperature data during the July 13, 1982, SPE, the largest of solar cycle 21, and observe no detectable temperature decrease at 0.4, 1, and 2 mbar, consistent with our reasoning.

We have also performed a calculation to determine the effect of ozone depletion on the ambient temperature field at 50 km. From Figures 2 and 4 it is clear that most of the ozone depletion occurs at SZA's greater than 70°. We used the energy relations in *Blake and Lindzen* [1973] and made the assumption that 10% of the ozone is depleted for SZA's greater than 70°, with 5% being depleted at SZA's less than 70°. We calculated that there would be at most of 1.1°K cooling for July 13 over the course of 24 hours when compared to a 24-hour period with no ozone depletion. This calculation represents an upper limit of the amount of ozone depletion during the July 13, 1982, SPE and also includes no increased heating effect due to the increased ultraviolet field from decreased ozone above. Therefore this calculation would overestimate the difference in temperature between a perturbed and an unperturbed day.

Reagan et al. [1981] calculated a temperature decrease of only 2.2°K at 50 km during the August 1972 SPE (which

produced ionization rates at least an order of magnitude larger than the July 13, 1982, SPE at 50 km). Our calculation of, at most, a 1.1°K temperature decrease at 50 km is certainly not unreasonable. The joule heating by the protons will also be negligible. *Banks* [1979] showed that even for the intense August 1972 SPE, there was less than 0.5°K/d joule heating for all altitudes below 60 km.

At altitudes higher than 50 km the cooling calculated is similar to that at 50 km. For example, at 55 km (~0.5 mbar) we calculate at most a 1.0°K cooling, and at 60 km (~0.3 mbar) we calculate at most a 1.6°K cooling. Other SPE's during solar cycle 21 were all smaller than the July 13, 1982, SPE; thus even smaller temperature perturbations would be predicted for these SPE's.

CONCLUSIONS

Ozone depletions associated with SPE's have now been observed in nine events: November 1969, January and September 1971, August 1972, June and August 1979, October 1981, and July 13 and December 8, 1982. Here and in an earlier paper [*McPeters et al.*, 1981], we used photochemical models to study the ozone change connected with several of these SPE's near the stratopause. In this paper we examined the behavior of ozone with two 1D models and have been able to isolate mechanisms responsible for ozone change between 45 and 60 km. At large SZA's the natural source of HO_x becomes less important and the SPE source of HO_x relatively more important. A larger ozone depletion is therefore predicted at most larger SZA's for a given altitude. Observations of ozone decrease have been used in our models to predict changes in ozone at lower altitudes. If the ozone is depleted above a certain altitude, then the photodissociation rates for O_2 and O_3 at the lower altitudes are increased, and ozone may be either depleted or enhanced. A depletion of 10.5% at 55-km altitude during the July 13, 1982, SPE is predicted from our 1D photochemical equilibrium model computation to result directly from this column O_3 decrease for an SZA of 88°. Subtle enhancements (self-healing) are predicted for extremely high SZA's at 45 and 50 km and appear to be verified by observations.

The SZA-dependent depletion is qualitatively reproduced by the models during the July 13, 1982, and December 8, 1982, SPE's. In most cases the total amount of ozone decrease observed by NIMBUS 7 (SBUV) is larger than that predicted by our models for altitude 50–60 km, even when the observed ozone depletions at higher altitudes are included in the models. The total amount of ozone decrease observed by SME is about the same as that predicted by our models for altitudes 50–60 km, when the observed ozone depletions are used to supplement the models. In spite of the differences between the observations from the two satellites, we can conclude that a totally self-consistent model predicts significantly less ozone depletion than that observed at 50 and 55 km. This failure may be related to the ozone balance problem noted recently in the literature [*Solomon et al.*, 1983c; *Crutzen and Schmailzl*, 1983] for these altitudes.

APPENDIX: ONE-DIMENSIONAL TIME-DEPENDENT MODEL

A unique type of 1D time-dependent model was used in this study. The 1D model was imbedded in the 2D model framework of *Guthrie et al.* [1984]. The 2D model uses a residual mean circulation approximated by the diabatic heating with a small amount of dissipative mixing everywhere. The 2D model domain is from −85 to +85° in latitude at 10° intervals and from the ground up to approximately 60 km in altitude (~0.23 mbar), with a vertical resolution of about 2 km as represented by 30 levels in log pressure coordinates.

The 2D model was run in a diurnal average mode for several years of model time with CH_4 and N_2O fixed to the NIMBUS 7 stratospheric and mesospheric sounder (SAMS) measurements [*Jones and Pyle*, 1984], Cl_x at the stratopause fixed at about 3 ppbv commensurate with the measurements of *Berg et al.* [1980], O_3 fixed to SBUV measurements [*McPeters et al.*, 1984], and H_2O fixed to be 6 ppmv from 3 mbar up to the top of model and tapering down to about 3 ppmv at the tropopause and then increasing again to reach $\sim 1 \times 10^4$ ppmv at the ground. These values are within the range given in *Ellsaesser* [1983], very close to NIMBUS 7 limb infrared monitor of the stratosphere (LIMS) measurements [*Russell et al.*, 1984] and are consistent with the H_2O expected, assuming 3 ppmv from methane oxidation and 3 ppmv from tropospheric upwelling.

Solution of the species at each grid point is the same as that described by *Guthrie et al.* [1984], and the reactions and rates used are given in Table A1. The photodissociation rates are calculated the same as in the 1D photochemical equilibrium model and are discussed in the next section of this appendix. The following species were calculated: O, $O(^1D)$, H, OH, HO_2, N, NO, NO_2, NO_3, N_2O_5, HNO_3, HO_2NO_2, H_2, Cl, ClO, HCl, HOCl, and $ClONO_2$. The species H_2 was assumed to have a boundary condition of 0.5 ppmv at the ground. After it was determined that the annual cycle for all species was repeating, the 2D run was stopped. All subsequent runs were done in a 1D sense, the diurnal cycle was allowed to proceed, and O_3 was added to the list of species to be calculated. The 1D model, using a latitude of 68.7° (which results in a maximum solar zenith angle of 89° for the July 13, 1982, SPE), was run until the diurnal cycle repeated from day to day for all species.

This particular 1D model has the advantage of having the transport set by a more realistic 2D model. Since the SPE's last from a few hours to a few days in most cases, the transport of species from one latitude grid point to another is presumed to be small in this 2D model framework. The O_3 at latitude grid points next to the latitude grid where the 1D model is computed are also set to observed values. The CH_4 which helps determine the partitioning among the various Cl_x species is fixed to measurements, and the N_2O, which is the major producer of NO_x in the stratosphere, is fixed to measurements. Since the SPE's studied occur at high latitudes in the summer, it is assumed that the NO_x flow down from the thermosphere is a small influence on the total NO_x in the upper stratosphere and lower mesosphere. Model calculations [*Solomon et al.*, 1982; *Frederick and Orsini*, 1982; *Garcia and Solomon*, 1983] indicate that NO_x downward transport from the thermosphere at the high latitudes will have significant effects in the upper stratosphere during the winter, but practically no effect will be observed during summer.

ONE-DIMENSIONAL PHOTOCHEMICAL EQUILIBRIUM MODEL

We constructed a 1D version of the photochemical equilibrium model described by *McPeters et al.* [1981]. No diffusion or transport were included in this model. This model contains O_3, O, $O(^1D)$, H, OH, HO_2, NO_2, Cl, and ClO self-consistently calculated in steady state given the species H_2O, NO, N_2, O_2, CH_4, HCl, and HOCl. The model atmosphere giving the N_2 and O_2 distribution is taken from the U.S. Standard Atmosphere Supplements (1966) for 60°N in July.

TABLE A1. Reactions and Their Rates

No.	Reaction	Reaction Rate
(R1)	$O_2 + h\nu \rightarrow O + O$	J_1
(R2)	$O_3 + h\nu \rightarrow O_2 + O$	J_2
(R3)	$O_3 + h\nu \rightarrow O_2 + O(^1D)$†	J_3
(R4)	$H_2O + h\nu \rightarrow H + OH$	J_4
(R5)	$NO_2 + h\nu \rightarrow NO + O$	J_5
(R6)	$HCl + h\nu \rightarrow H + Cl$	J_6
(R7)	$HOCl + h\nu \rightarrow OH + Cl$	J_7
(R8)	$NO + h\nu \rightarrow N + O$	J_8
(R9)	$NO_3 + h\nu \rightarrow NO_2 + O$	J_9
(R10)	$NO_3 + h\nu \rightarrow NO + O_2$	J_{10}
(R11)	$N_2O + h\nu \rightarrow N_2 + O(^1D)$	J_{11}
(R12)	$N_2O_5 + h\nu \rightarrow NO_2 + NO_2 + O$	J_{12}
(R13)	$HNO_3 + h\nu \rightarrow OH + NO_2$	J_{13}
(R14)	$HO_2NO_2 + h\nu \rightarrow HO_2 + NO_2$	J_{14}
(R15)	$ClONO_2 + h\nu \rightarrow Cl + NO_3$	J_{15}
(R16)	$O + O_2 + M \rightarrow O_3 + M$	k_{16} [see *NASA*, 1983]
(R17)	$O + O_3 \rightarrow O_2 + O_2$	$k_{17} = 8.0 \times 10^{-12} \exp(-2060/T)$
(R18)	$OH + O \rightarrow O_2 + H$	$k_{18} = 2.2 \times 10^{-11} \exp(117/T)$
(R19)	$OH + O_3 \rightarrow O_2 + HO_2$	$k_{19} = 1.6 \times 10^{-12} \exp(-940/T)$
(R20)	$HO_2 + O \rightarrow O_2 + OH$	$k_{20} = 3.0 \times 10^{-11} \exp(200/T)$
(R21)	$HO_2 + O_3 \rightarrow O_2 + O_2 + OH$	$k_{21} = 1.4 \times 10^{-14} \exp(-580/T)$
(R22)	$H + O_2 + M \rightarrow HO_2 + M$	k_{22} [see *NASA*, 1983]
(R23)	$H + O_3 \rightarrow OH + O_2$	$k_{23} = 1.4 \times 10^{-10} \exp(-470/T)$
(R24)	$OH + HO_2 \rightarrow O_2 + H_2O$	$k_{24} = 7.0 \times 10^{-11}$
(R25)	$NO_2 + O \rightarrow O_2 + NO$	$k_{25} = 9.3 \times 10^{-12}$
(R26)	$NO + O_3 \rightarrow O_2 + NO_2$	$k_{26} = 1.8 \times 10^{-12} \exp(-1370/T)$
(R27)	$O(^1D) + H_2O \rightarrow OH + OH$	$k_{27} = 2.2 \times 10^{-10}$
(R28)	$O(^1D) + N_2 \rightarrow O + N_2$	$k_{28} = 1.8 \times 10^{-11} \exp(107/T)$
(R29)	$O(^1D) + O_2 \rightarrow O + O_2$	$k_{29} = 3.2 \times 10^{-11} \exp(67/T)$
(R30)	$Cl + O_3 \rightarrow ClO + O_2$	$k_{30} = 2.8 \times 10^{-11} \exp(-257/T)$
(R31)	$ClO + O \rightarrow Cl + O_2$	$k_{31} = 7.7 \times 10^{-11} \exp(-130/T)$
(R32)	$OH + HCl \rightarrow H_2O + Cl$	$k_{32} = 2.8 \times 10^{-12} \exp(-425/T)$
(R33)	$Cl + HO_2 \rightarrow HCl + O_2$	$k_{33} = 1.8 \times 10^{-11} \exp(170/T)$
(R34)	$HO_2 + ClO \rightarrow HOCl + O_2$	$k_{34} = 4.6 \times 10^{-13} \exp(710/T)$
(R35)	$Cl + CH_4 \rightarrow HCl + CH_3$‡	$k_{35} = 9.6 \times 10^{-12} \exp(-1350/T)$
(R36)	$O(^1D) + N_2O \rightarrow N_2 + O_2$	$k_{36} = 4.9 \times 10^{-11}$
(R37)	$O(^1D) + N_2O \rightarrow NO + NO$	$k_{37} = 6.7 \times 10^{-11}$
(R38)	$O(^1D) + N_2 + M \rightarrow N_2O + M$	k_{38} [see *NASA*, 1983]
(R39)	$NO_2 + O_3 \rightarrow NO_3 + O_2$	$k_{39} = 1.2 \times 10^{-13} \exp(-2450/T)$
(R40)	$N + O_2 \rightarrow NO + O$	$k_{40} = 4.4 \times 10^{-12} \exp(-3220/T)$
(R41)	$N + NO \rightarrow N_2 + O$	$k_{41} = 3.4 \times 10^{-11}$
(R42)	$N + NO_2 \rightarrow N_2O + O$	$k_{42} = 3.0 \times 10^{-12}$
(R43)	$NO_3 + O \rightarrow NO_2 + O_2$	$k_{43} = 1.0 \times 10^{-11}$
(R44)	$NO + O + M \rightarrow NO_2 + M$	k_{44} [see *NASA*, 1983]
(R45)	$NO_2 + O + M \rightarrow NO_3 + M$	k_{45} [see *NASA* 1983]
(R46)	$NO_2 + O_3 \rightarrow NO_3 + O_2$	$k_{46} = 1.2 \times 10^{-13} \exp(-2450/T)$
(R47)	$NO_3 + NO_2 + M \rightarrow N_2O_5 + M$	k_{47} [see *NASA*, 1983]
(R48)	$NO_3 + NO \rightarrow NO_2 + NO_2$	$k_{48} = 2.0 \times 10^{-11}$
(R49)	$N_2O_5 + M \rightarrow NO_2 + NO_3 + M$	k_{49} [see *NASA*, 1983]
(R50)	$H + HO_2 \rightarrow H_2 + O_2$	$k_{50} = 7.0 \times 10^{-12}$
(R51)	$H + HO_2 \rightarrow OH + OH$	$k_{51} = 6.4 \times 10^{-11}$
(R52)	$H + HO_2 \rightarrow H_2O + O$	$k_{52} = 3.0 \times 10^{-12}$
(R53)	$H_2 + O(^1D) \rightarrow H + OH$	$k_{53} = 1.0 \times 10^{-10}$
(R54)	$H_2 + OH \rightarrow H + H_2O$	$k_{54} = 6.1 \times 10^{-12} \exp(-2030/T)$
(R55)	$OH + OH \rightarrow H_2O + O$	$k_{55} = 4.2 \times 10^{-12} \exp(-242/T)$
(R56)	$OH + HO_2 + M \rightarrow H_2O + O_2 + M$	k_{56} [see *NASA*, 1983]§
(R57)	$HO_2NO_2 + O \rightarrow OH + O_2 + NO_2$	$k_{57} = 7.0 \times 10^{-11} \exp(-3370/T)$
(R58)	$NO + HO_2 \rightarrow NO_2 + HO$	$k_{58} = 3.7 \times 10^{-12} \exp(240/T)$
(R59)	$HO_2NO_2 + OH \rightarrow H_2O + O_2 + NO_2$	$k_{59} = 1.3 \times 10^{-12} \exp(380/T)$
(R60)	$OH + HNO_3 \rightarrow H_2O + NO_3$	$k_{60} = 9.4 \times 10^{-15} \exp(778/T)$
(R61)	$HO_2NO_2 + M \rightarrow HO_2 + NO_2 + M$	k_{61} [see *NASA*, 1983]
(R62)	$NO_2 + HO_2 + M \rightarrow HO_2NO_2 + M$	k_{62} [see *NASA*, 1983]
(R63)	$OH + NO_2 + M \rightarrow HNO_3 + M$	k_{63} [see *NASA*, 1983]
(R64)	$ClO + NO \rightarrow Cl + NO_2$	$k_{64} = 6.2 \times 10^{-12} \exp(294/T)$
(R65)	$OH + HOCl \rightarrow H_2O + ClO$	$k_{65} = 3.0 \times 10^{-12} \exp(-150/T)$
(R66)	$Cl + HO_2 \rightarrow OH + ClO$	$k_{66} = 4.1 \times 10^{-11} \exp(-450/T)$
(R67)	$Cl + H_2 \rightarrow H + HCl$	$k_{67} = 3.7 \times 10^{-11} \exp(-2300/T)$
(R68)	$NO_2 + ClO + M \rightarrow ClONO_2 + M$	k_{68} [see *NASA*, 1983]
(R69)	$ClONO_2 + O \rightarrow ClO + NO_3$	$k_{69} = 3.0 \times 10^{-12} \exp(-808/T)$
(R70)	$ClONO_2 + OH \rightarrow HOCl + NO_3$	$k_{70} = 1.2 \times 10^{-12} \exp(-333/T)$

The reaction rates are taken from the *National Aeronautics and Space Administration* (NASA) [1983].
†Spin conservation is not violated. $O_2(^1\Delta)$ is assumed to quench to O_2 rapidly.
‡The product CH_3 is not a computed species.
§A pressure dependence is given in Table 1 of *NASA* [1983] for the $OH + HO_2$ reaction.

The CH_4 is taken from SAMS data [*Jones and Pyle*, 1984] and the HCl and HOCl distributions were taken from the 2D diurnal average model described earlier. The H_2O profile was set at 6 ppmv for the dynamic range of the model from altitudes 45 through 60 km (~2–0.3 mbar). The NO profile is taken from *Horvath et al.* [1983, Figure 3], which was a measurement at mid-latitude summer. The profile was extrapolated from 52 up to 60 km (~0.7 up to 0.3 mbar) following NO profiles derived for *Jackman et al.* [1980]. Table A2 presents these fixed species as functions of altitude.

Photodissociation rates were calculated using a method similar to the one used in our 1D time-dependent model described earlier and the 1D model of *Frederick et al.* [1983]. The photodissociation rates were calculated with cross sections recommended in the *National Aeronautics and Space Administration* [1983] report. The solar flux above the atmosphere was the same as that used in the 1D time-dependent model (described above). We use the solar flux measurements of *Mount and Rottman* [1981] for wavelengths shorter than 165 nm. Between 165 and 400 nm the flux used is given by D. F. Heath (private communication, 1981; see also *World Meteorological Organization* [1981]), and for wavelengths longer than 400 nm the flux is taken from the *World Meteorological Organization* [1981]. Scattering of sunlight is included using the two-stream radiative transfer method of *Herman* [1979], which extended from the ground to 90 km. For simplicity, an albedo of 0.25 was assumed at the ground for all wavelengths. An albedo much larger than 0.25 is not expected between 60° and 70° latitude in the summer. In the winter at these high latitudes, larger albedos are, of course, possible. The O_2 absorption cross sections recently derived by *Herman and Mentall* [1982] are used in the Herzberg continuum, while O_2 absorption cross sections given by the expressions in *Allen and Frederick* [1982] are used in the Schumann-Runge wavelength region. Ozone profiles up to 90 km were fixed at values given in Table A3 in the model to derive photodissociation rates as a function of altitude for the ambient atmosphere. These were taken from NIMBUS 7 (SBUV) and SME measurements. For some perturbed atmosphere runs the O_3 values were changed commensurate with observed O_3 decreases.

The reactions and rates used in this model are given in Table A1. For this model we use a subset of these rates, which includes reactions (R1)–(R7) and (R16)–(R35). In order to solve for each species the continuity equation

$$\frac{dn_i}{dt} = P(n_i) - L(n_i) \qquad \text{(A1)}$$

is set up. $P(n_i)$ and $L(n_i)$ are the production and loss rates, respectively, for the ith species. The assumption is then made that photochemical equilibrium exists for each species. The several analytical formulas relating each species to the others are solved using an iterative procedure until the densities for all species are unchanging to one part in a thousand from one iteration to the next.

TABLE A2. Temperature and Species Number Densities (cm^{-3}) or Mixing Ratios as a Function of Altitude Used in the One-Dimensional Photochemical Equilibrium Model

	45 km, 273.6°K	50 km, 277.2°K	55 km, 274.0°K	60 km, 262.7°K
Species				
N_2	3.76×10^{16}	2.01×10^{16}	1.11×10^{16}	6.20×10^{15}
O_2	1.01×10^{16}	5.41×10^{15}	2.97×10^{15}	1.66×10^{15}
H_2O, ppmv	6	6	6	6
NO, ppbv	12	15	16	16
CH_4, ppmv	0.24	0.14	0.10	0.06
HCl, ppbv	2.4	2.9	3.0	3.0
HOCl, ppbv	0.09	0.02	0.006	0.002

TABLE A3. Ozone Values (cm^{-3}) Used in Deriving Photodissociation Rates in the One-Dimensional Photochemical Equilibrium Model

Altitude, km	Ozone Density
45	1.11×10^{11}
50	5.70×10^{10}
55	1.74×10^{10}
60	6.21×10^{9}
65	3.36×10^{9}
70	1.12×10^{9}
75	2.94×10^{8}
80	9.05×10^{7}
85	6.69×10^{7}
90	5.21×10^{7}

Acknowledgments. The authors thank Susan Solomon of NOAA, Boulder, and Richard S. Stolarski of NASA Goddard for several useful discussions. D. Evans and H. Sauer of NOAA, Boulder, through Susan Solomon, kindly provided proton and electron flux data for the July 13 and December 8, 1982, SPE's. We appreciate this help. The authors also thank Anne R. Douglass of Applied Research Corporation, who provided use of a one-dimensional model to calculate photodissociation rates, Robert E. McGuire of NASA Goddard, who provided proton flux data for several other SPE's, Mao-Fou Wu of NASA Goddard and Jerry G. Olson of Applied Research Corporation for providing NMC temperature data, John E. Frederick of NASA Goddard for valuable suggestions concerning this manuscript, and Roberta M. Duffy of NASA Goddard for typing the manuscript.

REFERENCES

Allen, M., and J. E. Frederick, Effective photodissociation cross sections for molecular oxygen and nitric oxide in the Schumann-Runge bands, *J. Atmos. Sci.*, *39*, 2066–2075, 1982.

Banks, P. M., Joule heating in the high-latitude mesosphere, *J. Geophys. Res.*, *84*, 6709–6712, 1979.

Barnett, J. J., J. T. Houghton, and J. A. Pyle, The temperature dependence of the ozone concentration near the stratosphere, *Q. J. R. Meteorol. Soc.*, *101*, 245–257, 1975.

Berg, W. W., P. J. Crutzen, F. E. Grahek, S. N. Gitlin, and W. A. Sedlacek, First measurements of total chlorine and bromine in the lower stratosphere, *Geophys. Res. Lett.*, *7*, 937–940, 1980.

Blake, D., and R. S. Lindzen, Effect of photochemical models on calculated equilibria and cooling rates in the stratosphere, *Mon. Weather Rev.*, *101*, 783–802, 1973.

Climatic Impact Assessment Program, The natural stratosphere of 1974, CIAP Monogr. 1, *DOT-TST-75-51*, Dep. of Transp., Washington, D. C., 1975.

Crutzen, P. J., and U. Schmailzl, Chemical budgets of the stratosphere, *Planet. Space Sci.*, *31*, 1009–1032, 1983.

Crutzen, P. J., and S. Solomon, Response of mesospheric ozone to particle precipitation, *Planet. Space Sci.*, *28*, 1147–1153, 1980.

Ellsaesser, H. W., Stratospheric water vapor, *J. Geophys. Res.*, *88*, 3897–3906, 1983.

Frederick, J. E., Solar corpuscular emission and neutral chemistry in the earth's middle atmosphere, *J. Geophys. Res.*, *81*, 3179–3186, 1976.

Frederick, J. E., and N. Orsini, The distribution and variability of mesospheric odd nitrogen: A theoretical investigation, *J. Atmos. Terr. Phys.*, *44*, 479–488, 1982.

Frederick, J. E., F. T. Huang, A. R. Douglass, and C. A. Reber, The distribution and annual cycle of ozone in the upper stratosphere, *J. Geophys. Res.*, *88*, 3819–3828, 1983.

Garcia, R. R., and S. Solomon, A numerical model of the zonally averaged dynamical and chemical structure of the middle atmosphere, *J. Geophys. Res.*, *88*, 1379–1400, 1983.

Goldberg, R. A., C. H. Jackman, J. R. Barcus, and F. Sorass, Nighttime auroral energy deposition in the middle atmosphere, *J. Geophys. Res.*, *89*, 5581–5596, 1984.

Guthrie, P. D., C. H. Jackman, J. R. Herman, and C. J. McQuillan, A diabatic circulation experiment in a two-dimensional photochemical model, *J. Geophys. Res.*, *89*, 9589–9602, 1984.

Heath, D. F., A. J. Krueger, and P. J. Crutzen, Solar proton event: Influence on stratospheric ozone, *Science*, *197*, 886–889, 1977.

Herman, J. R., The response of stratospheric constituents to a solar eclipse, sunrise, and sunset, *J. Geophys. Res.*, *84*, 3701–3710, 1979.

Herman, J. R., and J. E. Mentall, O_2 absorption cross sections (187–225 nm) from stratospheric solar flux measurements, *J. Geophys. Res.*, *87*, 8967–8975, 1982.

Horvath, J. J., J. E. Frederick, N. Orsini, and A. R. Douglass, Nitric oxide in the upper stratosphere: Measurements and geophysical interpretation, *J. Geophys. Res.*, *88*, 10809–10817, 1983.

Hudson, R. D., (Ed.), Chlorofluoromethanes and the stratosphere, *NASA Ref. Publ. 1010*, 266 pp., 1977.

Hudson, R. D., and E. I. Reed (Eds.), *The Stratosphere: Present and Future*, *NASA Ref. Publ. 1049*, 1979.

Jackman, C. H., J. E. Frederick, and R. S. Stolarski, Production of odd nitrogen in the stratosphere and mesosphere: An intercomparison of source strengths, *J. Geophys. Res.*, *85*, 7495–7505, 1980.

Johnston, H. S., and J. Podolske, Interpretations of stratospheric photochemistry, *Rev. Geophys. Space Phys.*, *16*, 491–519, 1978.

Jones, R. L., and J. A. Pyle, Observations of CH_4 and N_2O by the NIMBUS 7 SAMS: A comparison with in situ data and two-dimensional numerical model calculations, *J. Geophys. Res.*, *89*, 5263–5279, 1984.

McPeters, R. D., and C. H. Jackman, The response of ozone to solar proton events during solar cycle 21: The observations, *J. Geophys. Res.*, this issue.

McPeters, R. D., C. H. Jackman, and E. G. Stassinopoulos, Observations of ozone depletion associated with solar proton events, *J. Geophys. Res.*, *86*, 12071–12081, 1981.

McPeters, R. D., D. F. Heath, and P. K. Bhartia, Average ozone profiles for 1979 from the NIMBUS 7 SBUV instrument, *J. Geophys. Res.*, *89*, 5199–5214, 1984.

Mount, G. H., and G. J. Rottman, The solar spectral irradiance 1200–3184 Å near solar maximum: July 15, 1980, *J. Geophys. Res.*, *86*, 9193–9198, 1981.

National Aeronautics and Space Administration, Chemical kinetics and photochemical data for use in stratospheric modeling, *NASA/JPL Publ. 83-62*, Jet Propul. Lab., Pasadena, Calif., 1983.

Nicolet, M., Stratospheric ozone: an introduction to its study, *Rev. Geophys. Space Phys.*, *13*, 593–636, 1975.

Reagan, J. B., R. E. Meyerott, R. W. Nightingale, R. C. Gunton, R. G. Johnson, J. E. Evans, W. L. Imhof, D. F. Heath, and A. J. Krueger, Effects of the August 1972 solar particle events on stratospheric ozone, *J. Geophys. Res.*, *86*, 1473–1494, 1981.

Russell, J. M., III, J. C. Gille, E. E. Remsberg, L. L. Gordley, P. L. Bailey, H. Fischer, A. Girard, S. R. Drayson, W. Evans, and J. E. Harries, Validation of water vapor results measured by the Limb Infrared Monitor of the Stratosphere (LIMS) experiment on NIMBUS 7, *J. Geophys. Res.*, *89*, 5115–5124, 1984.

Schoeberl, M. R., and D. F. Strobel, The zonally averaged circulation of the middle atmosphere, *J. Atmos. Sci.*, *35*, 577–591, 1978.

Smith, F. L., and C. Smith, Numerical evaluation of chapman's grazing incidence integral *ch*(*X*, *x*), *J. Geophys. Res.*, *77*, 3592–3597, 1972.

Solomon, S., and P. J. Crutzen, Analysis of the August 1972 solar proton event including chlorine chemistry, *J. Geophys. Res.*, *86*, 1140–1146, 1981.

Solomon, S., D. W. Rusch, J.-C. Gerard, G. C. Reid, and P. J. Crutzen, The effect of particle precipitation events on the neutral and ion chemistry of the middle atmosphere, 2, Odd hydrogen, *Planet. Space Sci.*, *29*, 885–892, 1981.

Solomon, S., P. J. Crutzen, and R. G. Roble, Photochemical coupling between the thermosphere and the lower atmosphere, 1, Odd nitrogen from 50 to 120 km, *J. Geophys. Res.*, *87*, 7206–7220, 1982.

Solomon, S., G. C. Reid, D. W. Rusch, and R. J. Thomas, Mesospheric ozone depletion during the solar proton event of July 13, 1982, 2, Comparison between theory and measurements, *Geophys. Res. Lett.*, *10*, 257–260, 1983*a*.

Solomon, S., G. C. Reid, D. W. Rusch, and R. J. Thomas, Mesospheric ozone depletion during solar proton events, paper presented at the Sixth ESA-PAC Meeting, Eur. Space Agency, Interlaken, Switzerland, April 12–19, 1983*b*.

Solomon, S., D. W. Rusch, R. J. Thomas, and R. S. Eckman, Comparison of mesospheric ozone abundances measured by the solar mesosphere explorer and model calculations, *Geophys. Res. Lett.*, *10*, 249–252, 1983*c*.

Swider, W., and T. J. Keneshea, Decrease of ozone and atomic oxygen in the lower mesosphere during a PCA event, *Planet. Space Sci.*, *21*, 1969–1973, 1973.

Swider, W., T. J. Keneshea, and C. I. Foley, An SPE-disturbed D-region model, *Planet. Space Sci.*, *26*, 883–892, 1978.

Thomas, R. J., C. A. Barth, G. J. Rottman, D. W. Rusch, G. H. Mount, G. M. Lawrence, R. W. Sanders, G. E. Thomas, and L. E. Clemens, Mesospheric ozone depletion during the solar proton event of July 13, 1982, 1, Measurement, *Geophys. Res. Lett.*, *10*, 253–255, 1983.

Weeks, L. H., R. S. CuiKay, and J. R. Corbin, Ozone measurements in the mesosphere during the solar proton event of November 2, 1969, *J. Atmos. Sci.*, *29*, 1138–1142, 1972.

World Meteorological Organization, The stratosphere 1981: Theory and measurements, *Rep. 11*, Ozone Res. Moniting Proj., Geneva, 1981.

C. H. Jackman and R. D. McPeters, NASA Goddard Space Flight Center, Atmospheric Chemistry and Dynamics Branch, Code 616, Greenbelt, MD 20771.

(Received June 28, 1984;
revised February 18, 1985;
accepted February 27, 1985.)